Bull Volcanol (2017) 79:58
DOI 10.1007/s00445-017-1138-4

RESEARCH ARTICLE

Eruptive and shallow conduit dynamics during Vulcanian explosions: insights from the Episode IV block field of the 1912 eruption of Novarupta, Alaska

S. J. Isgett[1] · B. F. Houghton[1] · S. A. Fagents[2] · S. Biass[1] · A. Burgisser[3] · L. Arbaret[4]

Received: 27 January 2017 / Accepted: 26 May 2017

Abstract The study of ~1300 juvenile and lithic blocks from a Vulcanian phase of the 1912 eruption of Novarupta provides new insight into the state of the magma as an eruption passes from sustained Plinian to dome growth. Blocks that were predominantly ballistically ejected were measured and sampled within an ~2–3-km radius from vent and supply a picture of a dynamic and complex shallow conduit prior to magma fragmentation in repeated small explosions. Extreme conduit heterogeneity is expressed in the diverse range of dacitic block types, including pumiceous, dense, banded, and variably welded breccia clasts, all with varied degrees of surface breadcrusting. We present new maps of block lithology and size, making Episode IV the most thoroughly mapped Vulcanian deposit to date. Sectorial regions rich in specific lithologies together with the block size data suggest multiple, small explosions. Modeling of block trajectories to reproduce the field data indicates that ejection velocities range from 50 to 124 m/s with a median of ~70 m/s. We propose that individual explosions originated from a heterogeneous shallow conduit characterized both by the juxtaposition of magma domains of contrasting texture and vesiculation state and by the intimate local mingling of different textures on short vertical and horizontal length scales at the contacts between these domains. In our model, each explosion disrupted the conduit to only shallow depths and tapped diverse, localized pockets within the conduit. This contrasts with existing models for repetitive Vulcanian explosions, and suggests that the dynamics of Episode IV were more complex than a simple progressive top-down evacuation of a horizontally stratified conduit.

Keywords Novarupta · Vulcanian explosions · Ballistic blocks · Shallow conduit architecture

Editorial responsibility: S. Self

Electronic supplementary material The online version of this article (doi:10.1007/s00445-017-1138-4) contains supplementary material, which is available to authorized users.

✉ S. J. Isgett
sweaver@hawaii.edu

[1] Department of Geology and Geophysics, SOEST, University of Hawai'i at Mānoa, 1680 East West Road, Honolulu, HI 96822, USA

[2] Hawai'i Institute of Geophysics and Planetology, University of Hawai'i at Mānoa, 1680 East West Road, Honolulu, HI 96822, USA

[3] Université Savoie Mont Blanc, CNRS, IRD, ISTerre, F-73376 Le Bourget-du-Lac, France

[4] Université d'Orléans, CNRS, ISTerre, 1A rue de la Férollerie, 45071 Orléans Cedex 2, France

Introduction

Vulcanian eruptions are short-lived, impulsive explosions that are generally episodic and unpredictable. The impacts of individual Vulcanian explosions are typically less devastating than their larger, steady, and sustained explosive counterparts, yet they are much more common and can pose protracted risks when they occur in sequences lasting weeks to decades. Vulcanian explosions last seconds to minutes and evacuate only a portion of the magma resident in the upper conduit, producing small volumes of <0.1 km^3 dense rock equivalent (DRE). The resulting short-lived plumes typically reach heights of <10 km and may collapse to form pyroclastic density currents (Clarke et al. 2002b; Clarke 2013). A striking feature of many Vulcanian deposits is an abundance of highly diverse juvenile pyroclasts in varying proportions and textures. In a single eruption, pyroclasts may range between dense and highly vesicular and from microlite-free to microlite-rich (Adams et al. 2006a; Clarke et al. 2007; Wright et al. 2007; Cassidy et al. 2015).

Published online: 12 July 2017

The best-studied recent Vulcanian eruptions involved short, more intense intervals of explosive activity during long-lived dome-building eruptions (Melnik and Sparks 1999; Druitt et al. 2002; Kennedy et al. 2005; Scheu et al. 2006, 2008; Clarke et al. 2007; Burgisser et al. 2010; Giachetti et al. 2010). However, Vulcanian behavior can mark the opening stages of larger, sustained sub-Plinian or Plinian eruptions, such as during the 1991 eruption of Mount Pinatubo, Philippines (Hoblitt et al. 1996), or provide a transition from sustained powerful explosions to lava effusion as it did during 1980–1982 at Mount St. Helens, USA (Christiansen and Peterson 1981). At Soufrière Hills volcano, Vulcanian explosions during 1997 comprised short sequences of explosions that were part of longer-lived dome growth and collapse (Druitt et al. 2002). Smaller Vulcanian explosions can also occur daily over prolonged periods throughout decades-long dome-building eruptions, such as the 1929–present eruption of Volcán Santiaguito, Guatemala (Sahetapy-Engel et al. 2008).

Field observations such as ballistic range and clast size and density have been used to estimate eruptive conditions during transient explosions using models that apply the equations of motion and drag relationships. Early models assumed that pyroclasts were ejected into a stationary atmosphere resulting in an overestimation of the atmospheric drag force early in the explosion and unrealistically high ejection velocities (Minakami 1942; Fudali and Melson 1971; Wilson 1972). More sophisticated computational schemes have been developed over the last three decades in an attempt to account for changes in the drag force due to moving volcanic and atmospheric gases (Fagents and Wilson 1993; Waitt et al. 1995; Mastin 2001; Alatorre-Ibargüengoitia and Delgado-Granados 2006; de' Michieli Vitturi et al. 2010; Alatorre-Ibargüengoitia et al. 2010, 2012; Benage et al. 2014; Bertin 2017) and have yielded velocities closer to those estimated from image analysis.

Our current understanding of the initiation of Vulcanian events is firmly tied to models of such systems involving cyclic dome growth, development of a dense outgassed region in the upper conduit, conduit pressurization, dome disruption, fragmentation and conduit evacuation, and finally conduit refill (Druitt et al. 2002; Diller et al. 2006; Burgisser et al. 2010; Clarke 2013; Clarke et al. 2015). In such models, Vulcanian eruptions are the consequence of the sudden downward decompression of a conduit containing pressurized, horizontally stratified, rheologically heterogeneous magma in varying states of degassing and outgassing (Self et al. 1979; Turcotte et al. 1990; Fagents and Wilson 1993; Woods 1995; Clarke et al. 2002a, 2002b).

The variety of pyroclast densities and textures produced in Vulcanian explosions associated with large Plinian eruptions hints at a more complex conduit architecture than a simple horizontal layering (Adams et al. 2006a) and contrasts with the simple pyroclast textures seen in the associated Plinian phases. Opportunities to study the degree of this complexity, and how it influences the style of the overall eruption, are limited. Products of Episode IV of the 1912 eruption of Novarupta provide a unique opportunity to assess conduit complexity as the deposits are exceptionally well preserved. The Novarupta eruption consisted of five episodes ranging from strong Plinian (mass eruption rates of $1.1–5 \times 10^8$ kg/s) to dome effusion (Fierstein and Hildreth 1992; Hildreth and Fierstein 2000; Houghton et al. 2004; Adams et al. 2006b; Nguyen et al. 2014). Sixty hours of Plinian explosions erupted first predominantly rhyolite (early Episode I) and then dacite with minor amounts of andesite (Episodes II–III). Episode IV produced a dacitic block bed, interpreted as the product of complete destruction of a dacite plug/dome via Vulcanian explosions, before extrusion of a rhyolite dome in Episode V (Hildreth and Fierstein 2000; Houghton et al. 2004; Adams et al. 2006a). There were no direct observations of any part of the Novarupta eruption, only of events that affected surrounding communities such as earthquakes and ash/lapilli fall (Hildreth and Fierstein 2012). Without direct observations, durations and other source parameters for Episodes IV and V are unknown and we are dependent on the deposits for further understanding.

Compensatory caldera collapse during the Plinian episodes occurred 10 km from vent, preserving the ultra-proximal deposits from Episodes I through IV to within 200 m from source. The Episode IV block and lapilli apron that caps the fine ash from the close of Episode III is the only evidence that a dacite plug/dome formed at this time. The Episode IV deposit permits us to investigate the processes involved in the decline of a voluminous Plinian eruption during the transition from powerful, sustained explosive activity to stable extrusion of a lava dome. We can also contrast Episode IV with well-documented Vulcanian explosions during recent dome-building eruptions elsewhere, and address questions such as the following: what were the physical states, and their proportions, of the magma in the conduit; and did a single event destroy the plug/dome or did it involve a series of explosions?

Methodology

A total of 639 blocks was added to an existing data set (Adams et al. 2006a) yielding a new total of 1273 mapped blocks (Fig. 1). The largest blocks within 20–60-m-wide square areas at any distance and azimuth from the vent were located with a handheld GPS. Lithology, textures (including breadcrust rinds), and the three largest orthogonal dimensions were recorded, and an average dimension was calculated from the measurements. Fragments of blocks that broke apart upon

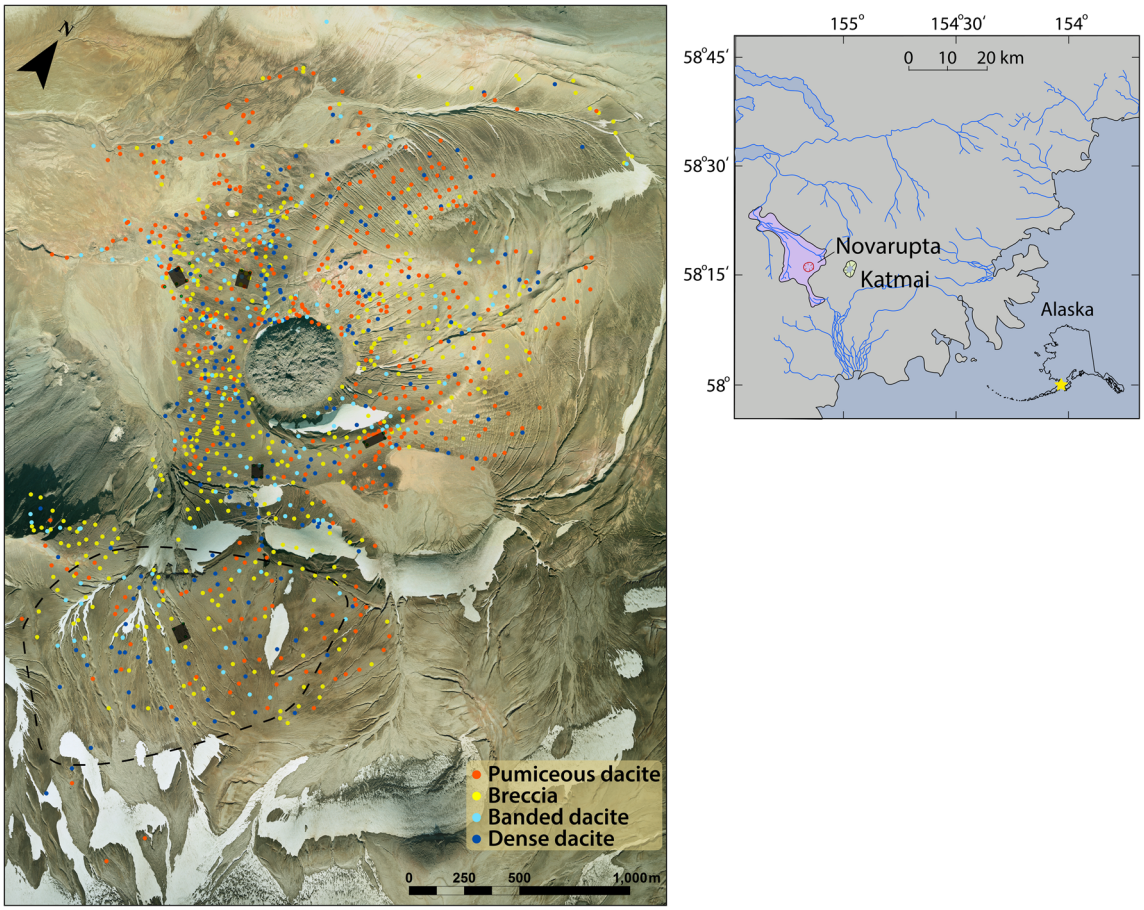

Fig. 1 *Left*, distribution of the Episode IV blocks according to lithology. *Black regions* are locations for the componentry quantification. *Black dashed line* delineates the area overlapping with the Episode IV block apron that contains dense andesites from the 1953 to 1974 eruptions of Southwest Trident volcano. *Round feature* in *middle* is the Episode V rhyolite dome. *Right*, location map for the 1912 deposits, including the Valley of Ten Thousand Smokes (in *purple*) and the Episode V dome (in *red*). *Yellow star* in *bottom right* denotes the location within Alaska. Figure modified after AVO/ADGGS

landing and could not be reassembled were piled up, and average dimension was estimated using the scaling factor of Adams et al. (2006a). A separate componentry quantification was conducted in five areas chosen for their density of blocks, remoteness from post-eruptive channels, and representative radial direction from the dome (black areas in Fig. 1). Two areas northwest of the Episode V dome were mapped by Adams et al. (2006a), and three areas in the south and southeast were measured in this study; the region northeast of the dome is not represented because of the steep slopes beneath the 1912 ejecta in this area. The 100 largest blocks (regardless of distance from one another) were measured along parallel transects within each area in order to ensure that the proportions of each component were accurately represented. Block densities were measured for a representative number of clasts within each componentry group, and an average density was calculated per group and applied to blocks that were not sampled.

Maps of block distribution according to (i) lithology and (ii) average dimension were constructed in ArcGIS. Note that these maps do not necessarily show the distributions of every large block on the ground surface. For example, if the largest block size is 50 cm (average dimension), then any blocks <50 cm within a 20–60-m square were not mapped. Care was taken to measure only blocks that were preserved in situ. This explains the reduced number of data points along steep slopes and the major gaps in the regions to the east (a seasonal lake bed) and southwest (a fluvial pumice delta) of the Novarupta dome on our maps.

Individual block trajectories were simulated using the algorithm of Fagents and Wilson (1993) to estimate initial ejection angles and velocities. Due to the difficulty of constraining the necessary conduit parameters for a detailed description of the drag regime close to the vent (e.g., conduit radius, gas volume fraction), we assume the ejection of blocks into a still atmosphere. We estimated the threshold, in terms of size and density, at which blocks could be treated as ejected into a stationary atmosphere, versus those blocks that were influenced by motions of the ambient (volcanic plus atmospheric) gases. This enabled a narrowing of the results down to the

most likely eruptive conditions during Episode IV. A detailed description of the equations of motion is presented in the Online Resource.

Block data

Episode IV block componentry

Clasts forming the texturally diverse and chemically homogeneous block apron were categorized into the lithologic groups assigned by Adams et al. (2006a). The majority of blocks are textural variations on phenocryst-rich dacite, and less than 1% include a pumiceous andesite component. Dacites were classified as pumiceous dacite, dense dacite, banded dacite, or breccia. Within each lithologic group, breadcrusting may be present or absent.

The pumiceous dacites are highly vesicular (average of 67%; Fig. 2) and the dominant lithology in the field (Fig. 3). Non-breadcrusted pumices are microvesicular with textures very similar to the Episode III Plinian pumices. Dense dacites are crystal-rich and vesicle-poor (Fig. 2), with 9% average vesicularity, and are the second least abundant lithology by volume. Their vesicle population is not visible to the naked eye. A number of dark, crystal-rich, dense blocks in a restricted area between West Trident and Novarupta basin (within the dashed line in Fig. 1) appear similar to the Novarupta dense dacites; however, they are andesites from the 1953–1974 eruptions of Southwest Trident volcano (Coombs et al. 2000).

Banded blocks exhibit sharp textural banding of juvenile dense and pumiceous dacite and were subdivided into three categories based on the relative proportions of each texture. A spectrum of flow banding types is present ranging from dominantly dense dacite (dense banded) to dominantly pumiceous dacite (pumiceous banded), and end-member vesicularities are 33 and 63%, respectively (Fig. 2). Other banded clasts contain subequal amounts of dense and pumiceous dacite (mixed banded), in often sharply delineated bands. Banding may be on a millimeter or centimeter scale or both, and bands may show plane-parallel contacts to their neighbors or pinch and swell. Strikingly, banding extends into rinds of breadcrusted samples (Fig. 2).

Breadcrusting, a variably cracked, quenched rind that generally is denser than the interior, is present on examples of all the lithologies, but especially on banded and pumiceous blocks (Figs. 2 and 4). Breadcrusting is more prevalent among the largest pumices but not for the dense dacites or breccias (Fig. 5). Rind vesicularity ranges from microvesicular but dense pumice to material that resembles dense dacite. The interiors of breadcrusted pumices are microvesicular but have significant numbers of centimeter-sized vesicles. There is always a gradual increase in number and size of the largest bubbles towards the block interior. Rind thickness is directly correlated with the density contrast between crust and interior.

Fig. 2 Clast lithologies observed within the Episode IV block field. **a** Non-breadcrusted pumice, N406. **b** Dense dacite, B126. **c** Breadcrusted dense banded; note that this block has millimeter-scale banding and consists of dominantly darker gray, denser bands with lighter gray, lower-density laminae, N113. **d** Pumiceous banded with overall beige pumiceous texture and light gray slightly denser bands, N322. **e** Mixed banded with bands of varying shades of gray and densities; note how the banding extends into the thin crusts on the outside edges of the flat faces, N197. **f** Breadcrusted mixed banded block with subequal amounts of centimeter/decimeter-thick dense and eroded pumice bands, B349. **g**, **h** Samples from block B349; note how the centimeter-thick dense and pumiceous bands contain laminae of different densities. Banding can be seen extending into the crust (*left side* of picture in **g** and at *top* of picture in **h**) in the form of darker/slightly more vesiculated crust that expands into interior pumice (*red arrow* in **h**). **i** Lightly welded breccia; weathering of the red oxidized and friable ashy matrix has formed a textured surface of outcropping pumice, B297. **j** Moderately welded breccia, B51. **k** Densely welded breccia, N038. **l** *Inset* of **k** highlighting the flattened pumice. **m** Dense vitrophyre with oxidized red lithics, N305

Breccias are of two types. The dominant breccia type (31% by volume) consists of dacitic pyroclasts and little or no wall rock in an ash matrix and exhibits a range of welding in the form of degree of pumice flattening and welding of the ash (Fig. 2). Lightly welded breccias have an average density of 1600 kg/m^3 and are characterized by equant dacite pumices in a friable ashy matrix. The moderately welded breccias are defined by a welded matrix showing clear pyroclast outlines with moderate flattening ratios averaging 3:1 and an average density of 1950 kg/m^3. The lithic-free dense breccias have an average density of 2200 kg/m^3, a crystal-rich, vitroclastic matrix, and pumice flattening of 5:1 to 7:1. Breadcrusting is present in a small proportion of these blocks. A second, subordinate category of breccias includes densely welded blocks containing pumice and pre-1912 Jurassic siltstone wall rock lithics, which are commonly oxidized brick red, set in a dark gray or black obsidian-like matrix (Fig. 2). They also occur in the Episodes II and III Plinian fall deposits and were inferred by Hildreth (1987) to be vitrophyric breccias formed in the Episode I vent. These breccias will be referred to as "dense vitrophyre" for the rest of this paper.

Block distribution by lithology and size

Adding our observations to those of Adams et al. (2006a) makes Episode IV globally the most comprehensively mapped Vulcanian block field (Nairn and Self 1978; Yamagishi and Feebrey 1994; Waitt et al. 1995; Druitt et al. 2002). We mapped the block distribution in terms of lithology and size (i.e., average dimension of the whole or reconstructed block), revealing a roughly N-S elongated elliptical deposit in which block size diminishes radially with distance from vent.

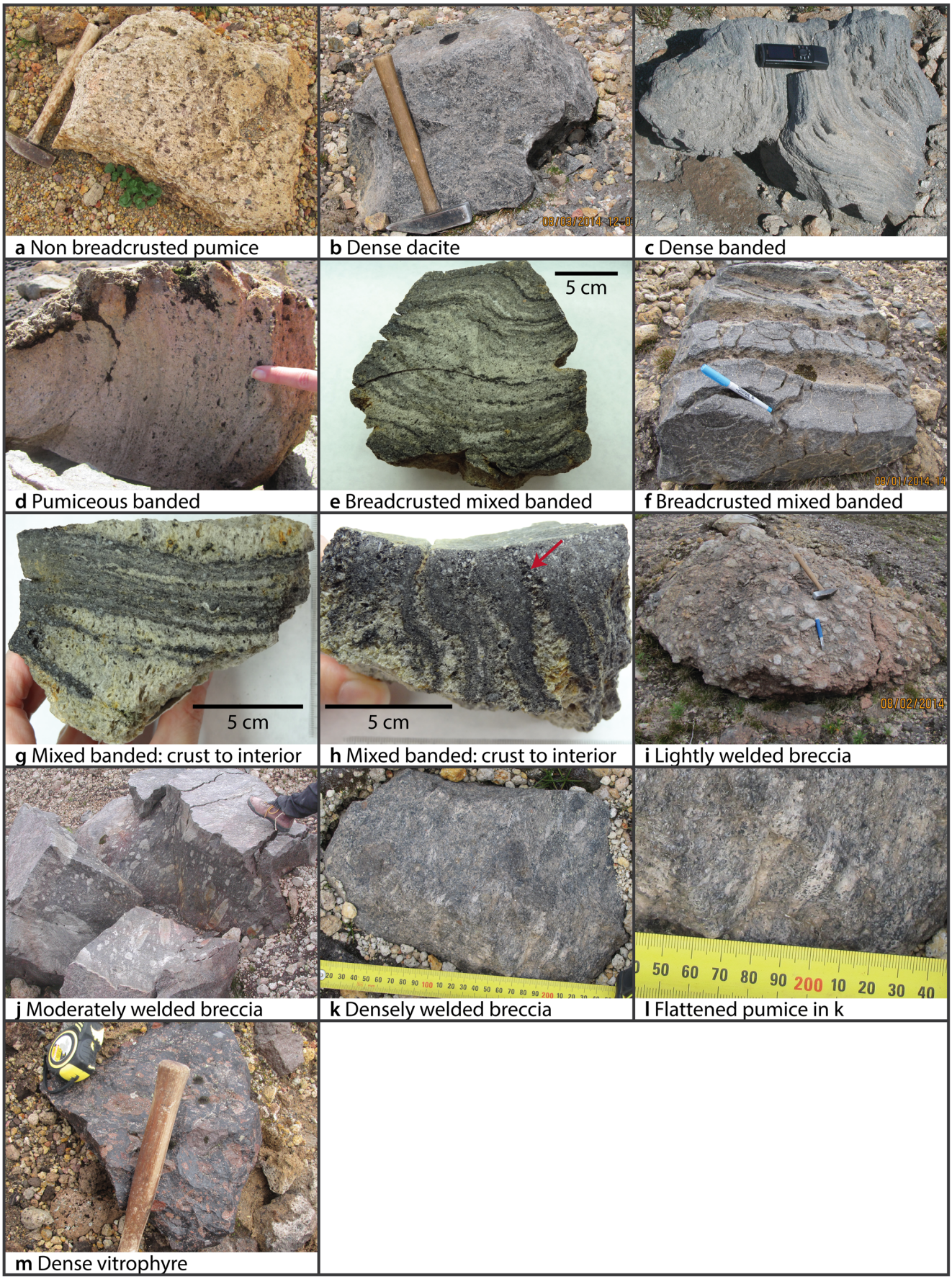
a Non breadcrusted pumice
b Dense dacite
c Dense banded
d Pumiceous banded
5 cm
e Breadcrusted mixed banded
f Breadcrusted mixed banded
5 cm
5 cm
g Mixed banded: crust to interior
h Mixed banded: crust to interior
i Lightly welded breccia
j Moderately welded breccia
k Densely welded breccia
l Flattened pumice in k
m Dense vitrophyre

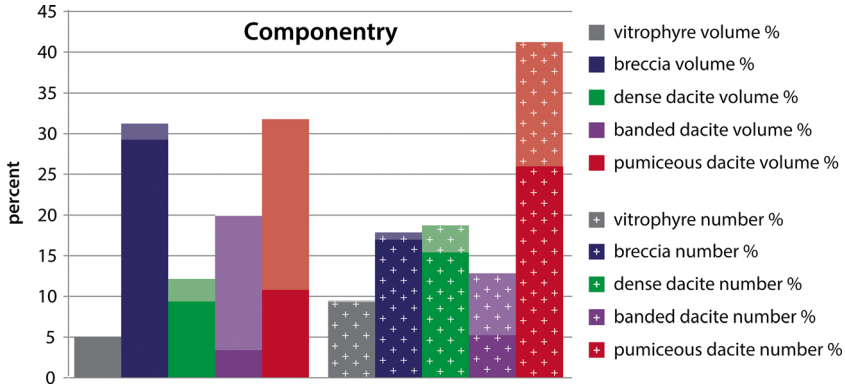

Fig. 3 Proportions of each component according to volume (*left*) and number (*right*). Each column is separated into lighter breadcrusted and darker non-breadcrusted proportions. The breccias and pumices are the most dominant according to volume, and the pumice blocks are 20% more numerous than any other lithology. The pumice and banded blocks are significantly more breadcrusted than the breccias and dense dacites

The spatial distribution of blocks suggests preferential clustering along a few radial axes (Fig. S1 in the Online Resource). In particular:

- *Dense dacites* are present radially within 600 m of vent (which lies beneath the Episode V dome) and are particularly abundant to the northwest to west and southwest to south. At distances >600 m, the dense dacites are weakly and unevenly concentrated to the north and south and are sparse to the east and west.
- *Pumiceous dacites* have a relatively even distribution to the north, east, and west and are moderately sparse south of the dome.
- *Episode I dense vitrophyres* are mostly strongly concentrated in the northeast, with weaker dispersal north, west, and south of the dome.
- *Densely welded breccias* are present in all radial directions within 600 m of vent, but are conspicuously richer in the south and absent from the north at distances >600 m.
- *Moderately welded breccias* are distributed in all sectors within 800 m of vent, and are particularly densely concentrated in the northwest to west and southwest to south quadrants. They are also noticeably absent to the north and present at greater distances to the south.
- *Lightly welded breccias* are concentrated in the west and northeast sectors with a weaker dispersal to the south and are nearly absent north of the dome.
- *Pumiceous banded clasts* have concentrations to the west, east, and southeast and are fairly sparse in the other sectors.
- *Mixed and dense banded clasts* have similar dispersals with stronger concentrations in the northwest to west and southwest to south sectors. They have only a minor presence to the northeast and are conspicuously absent directly north of the dome.

In summary, only the dense dacites and the densely and moderately welded breccias have a consistent presence in all sectors (to within 600 m) around the vent. The pumiceous dacites have a distinct concentration in the northwest to northeast sectors which is not present for the other lithologies. The remaining lithologies have sectoral confined distributions that usually (vitrophyre excluded) include more southerly (rather than northerly) distribution.

Figures 6 and 7 are isopleth maps for groups of lithologies with closely overlapping density distributions. These maps show proximal polylobate contours for the largest clasts and a smoothing of the smaller blocks' isopleths. The number, geometry, size distribution, and orientation of the lobes are correlated to block density. Higher densities produced lobes extending the farthest and to a smaller size fraction. The denser lithologies have six narrow lobes in the western and southern sectors whereas the lower-density components have fewer (five pumice, four banded, and three breccia) and broader

Fig. 4 **a** Breadcrusted moderately welded breccia, B347. **b** Breadcrusted pumiceous dacite, N332. **c** Cross section of a breadcrusted pumiceous dacite; note the gradational change in color reflecting an increase in bubble size and number towards the interior, N120

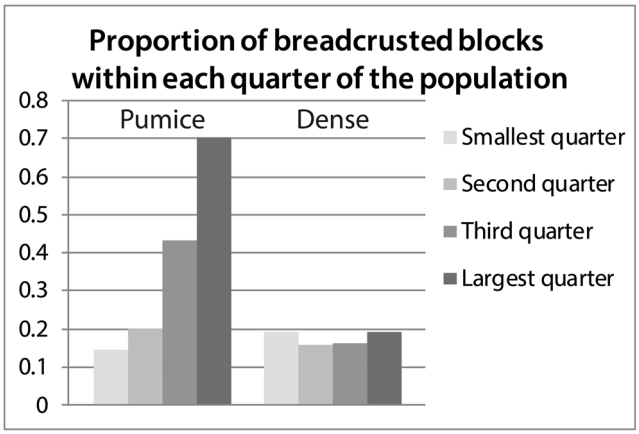

Fig. 5 Plot of the proportion of breadcrusted pumice (*left*) and dense dacite (*right*). Each lithology's block population was ordered by increasing average dimension and divided into quarters. The proportion of breadcrusted blocks was then calculated for each quarter. Note how the proportions of breadcrusted pumices increase with increasing block size whereas the dense dacites show no correlation between block size and the presence of breadcrusting

lobes that point towards the NW, SW, SE, NE, and N. The northern sector is characterized by a conspicuous absence of larger blocks and only one well-defined pumice lobe.

The overlap in 125- and 100-cm contours in Fig. 7 shows how distributions of different block types coincide in the northern sector. This contrasts with individually directed lobes towards the south of the dome. A broadening of fingers with decreasing block size results in a loss of distinct directionality especially in the southern sector, as is evident in the overlapping of fingers in the 75-cm contours.

Regardless of lithology or density, there is a general trend for block size to decrease with distance from the vent (Table 1; Fig. 8). However, the spread in block sizes reaching a given distance suggests that this correlation is associated with a large uncertainty. For example, block sizes present at a distance of 500 m in Fig. 8 range between 25 and 120 cm.

Block trajectory modeling results

General features

Initial conditions were estimated with the trajectory tracking model of Fagents and Wilson (1993) for 1269 blocks by incrementally cycling through ranges of ejection velocities (between 10 and 600 m/s) and launch angles (between 45 and 89° from horizontal) to find the combinations that reproduced observed block ejection distances within a buffer of ±10 m. Solutions were found for 972 blocks, while the remaining 297 (i.e., 23%) required implausibly high ejection velocities (greater than the 600-m/s limit set within the model). The majority of these 297 blocks were small (<50 cm diameter) and pumiceous (i.e., low-density), and landed >500 m from vent (Fig. 8). Few higher-density blocks gave unreasonable results, and nearly all that did landed >1 km from vent; the three exceptions were particularly small with average dimensions ≤20 cm.

To analyze the model results, the blocks were split into low-density (<1000 kg/m^3), intermediate-density (1000–<2000 kg/m^3), and high-density (≥2000 kg/m^3) groups and block size classes of small (<50 cm), medium (50–<100 cm), and large (≥100 cm) average dimension. Figure 9 displays the complete modeling results for these nine subclasses. Each curve represents model results for one block, i.e., all combinations of ejection velocity and angle that produce the measured travel distance for that block.

Clast diameter has a much more significant influence on the model results than clast density. For all three density classes, the largest blocks group tightly in Fig. 9 and the inferred velocity is relatively insensitive to ejection angle up to 70°–75° from horizontal. Beyond 70°–75°, model velocities increase steeply with ejection angle. For intermediate-sized blocks, velocities are more scattered and higher velocities are required at relatively shallow angles (55°–65°). These trends are even more apparent in the wide scatter of results for the smallest blocks.

Median velocity

We use the modeled velocities for an ejection angle of 45° to compare both median velocities and velocity ranges among the nine subclasses (Table 2). Median velocity increases (from ~70 to >150 m/s) as block size decreases. There is no simple relationship between median velocity and clast density.

Spread in velocity

The range in modeled velocity, represented by the separation of the 5th and 95th percentiles (range 2 in Table 2), narrows with increasing block size, from >350 m/s in the <50-cm size class to 60–70 m/s in the ≥100-cm size. No consistent relationship exists between density and the spread in velocity.

Dependence of ejection velocity on launch angle

Across all size classes, velocity is initially consistent across a range of angles and subsequently increases sharply for the steepest angles. This sharp increase occurs at lower angles for smaller blocks (Fig. 9), reducing the range of angles across which velocity is close to constant. For the smallest clasts, high ejection angles are not feasible at even extreme ejection velocities. Also note how the velocity range in each class widens as angle increases.

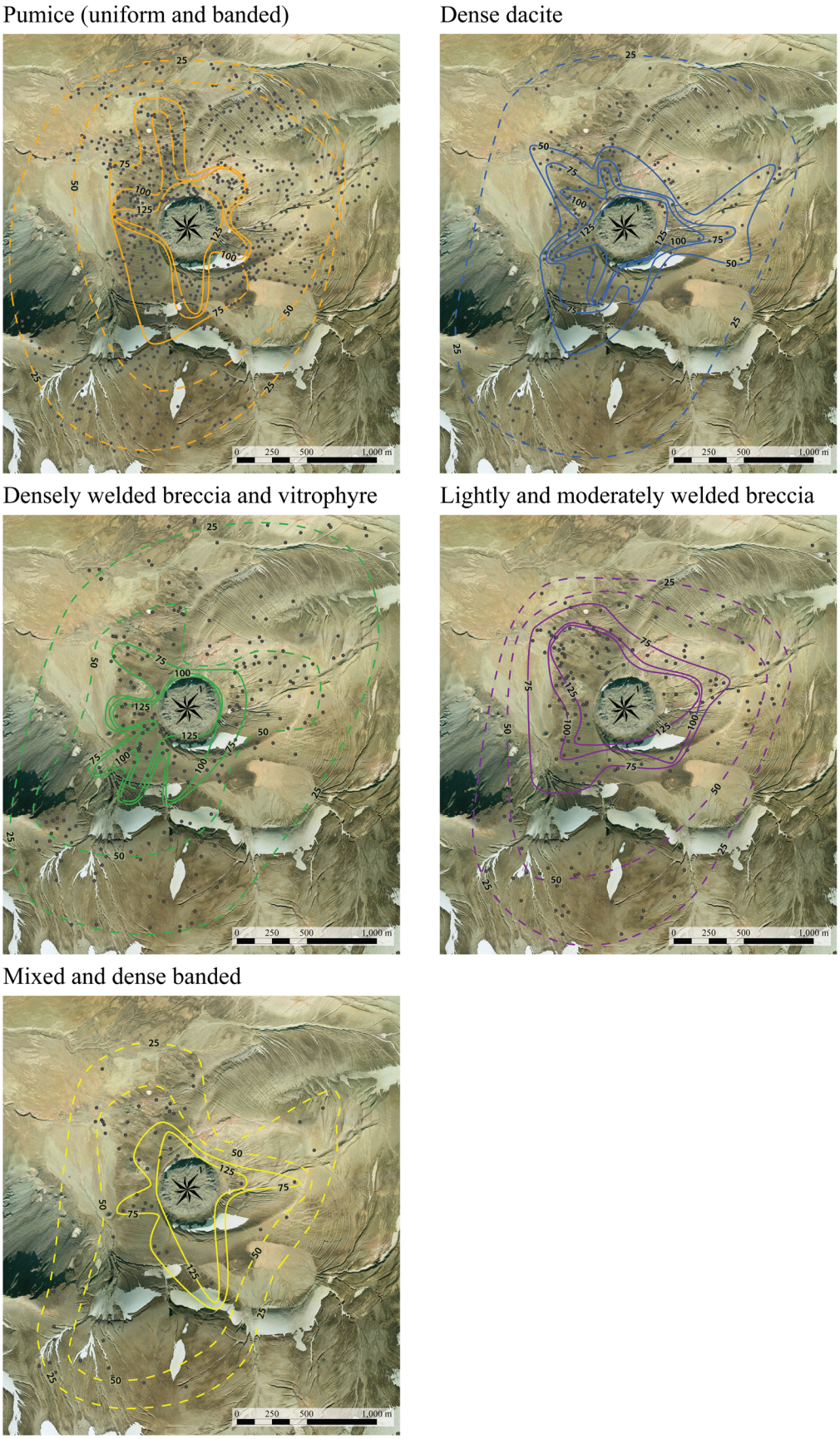

Fig. 6 Isopleth maps for the component groups

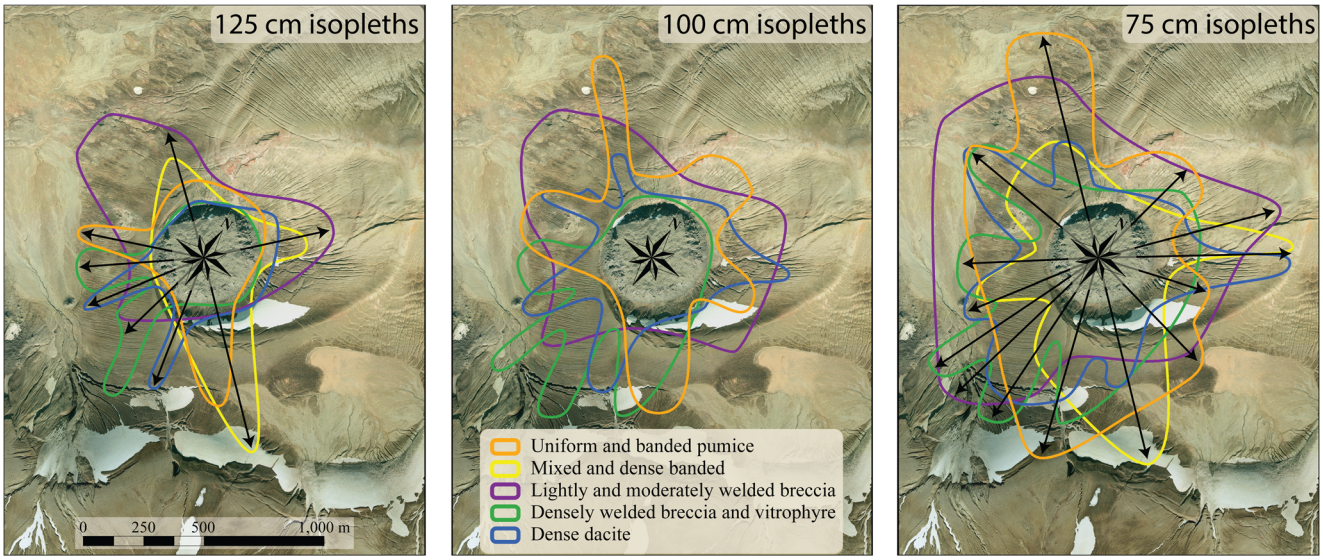

Fig. 7 Maps of overlapping isopleths of a single size from different lithological groups. *Arrows* indicate directed lobes within the deposits

Velocity versus distance

Given that the ejection velocity is relatively insensitive to a range of plausible ejection angles, the relationship between ejection velocity and landing distance is assessed in Fig. 10 for an ejection angle of 45°. The dataset for each size/density class is fit by a linear function and shown with the 95% confidence intervals. For comparison, we have also included a gray-shaded region in all plots that represents the 90% confidence interval of a linear fit performed on all blocks with diameters >1 m (i.e., bottom row of Fig. 10). First, these plots emphasize that the smallest blocks covered a wider spread of landing distances and required an unreasonably high and broad range in velocities across all densities. Note that a significant proportion of the low-density, <50-cm population is not represented in Fig. 10 because the model could not replicate their landing distances with any realistic ejection velocities (Fig. 8). Second, these plots show that velocity is predictably higher for the large blocks that traveled further. Finally, lower-density blocks require higher exit velocities to achieve any given distance in the small- and intermediate-size classes.

Interpretations

Block componentry interpretations

The distinct textural types among the clasts within Episode IV are chemically identical and probably reflect contrasting degrees of vesiculation at the time of fragmentation. Breadcrusting indicates that the exteriors of some blocks had solidified prior to interior vesiculation reaching equilibrium. Fine-scale flow banding of the range of physically distinct dacite types (e.g., dense/dense, pumiceous/pumiceous, pumiceous/dense; Fig. 2) suggests complex and intimate mingling, on length scales of millimeters to centimeters, of magma that had undergone different amounts of degassing and probably outgassing within the conduit. It means that mingling occurred at a very late stage and that insufficient time elapsed between mingling and eruption for diffusion of volatiles, thus precluding complete mixing of the disparate melts.

Block distribution interpretations

The pattern of isopleths shown in Figs. 6 and 7 is not easily reconciled with a simple deposit from a single explosion.

Table 1 Minimum, maximum, and the range of distances that the largest and smallest blocks traveled. Note how smaller blocks traveled further and cover a much wider range of distances, regardless of density

Density group (kg/m^3)	Block size (cm)	Minimum distance (m)	Maximum distance (m)	Range (m)
<1000	≥100	190	818	628
	<50	329	2423	2094
1000–<2000	≥100	206	902[a]	696
	<50	301	1791	1490
≥2000	≥100	204	942[b]	738
	<50	295	2264	1969

[a] Outlier maximum of 1052 m

[b] Outlier maximum of 1286 m

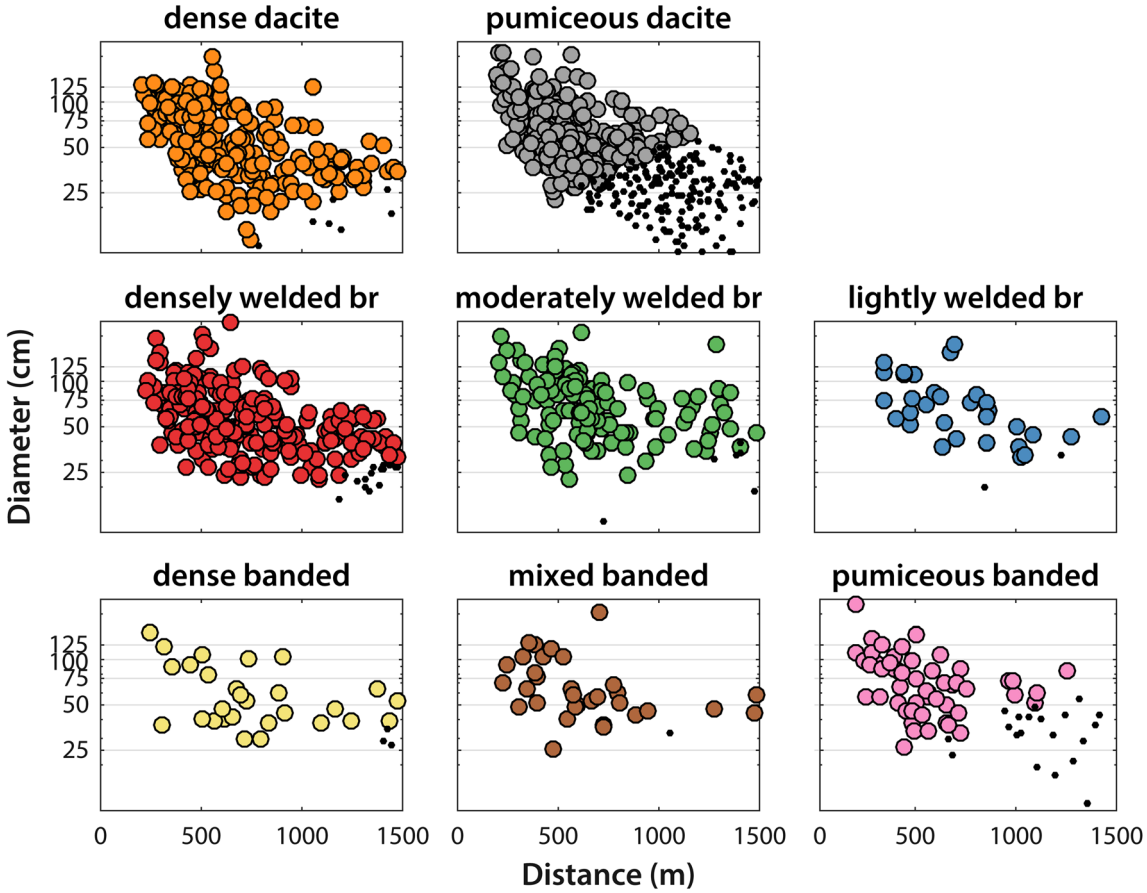

Fig. 8 Average diameter versus distance for each of the lithologies (*br* = breccia). *Black dots* represent blocks for which launch velocity exceeded the 600-m/s upper limit set within the model

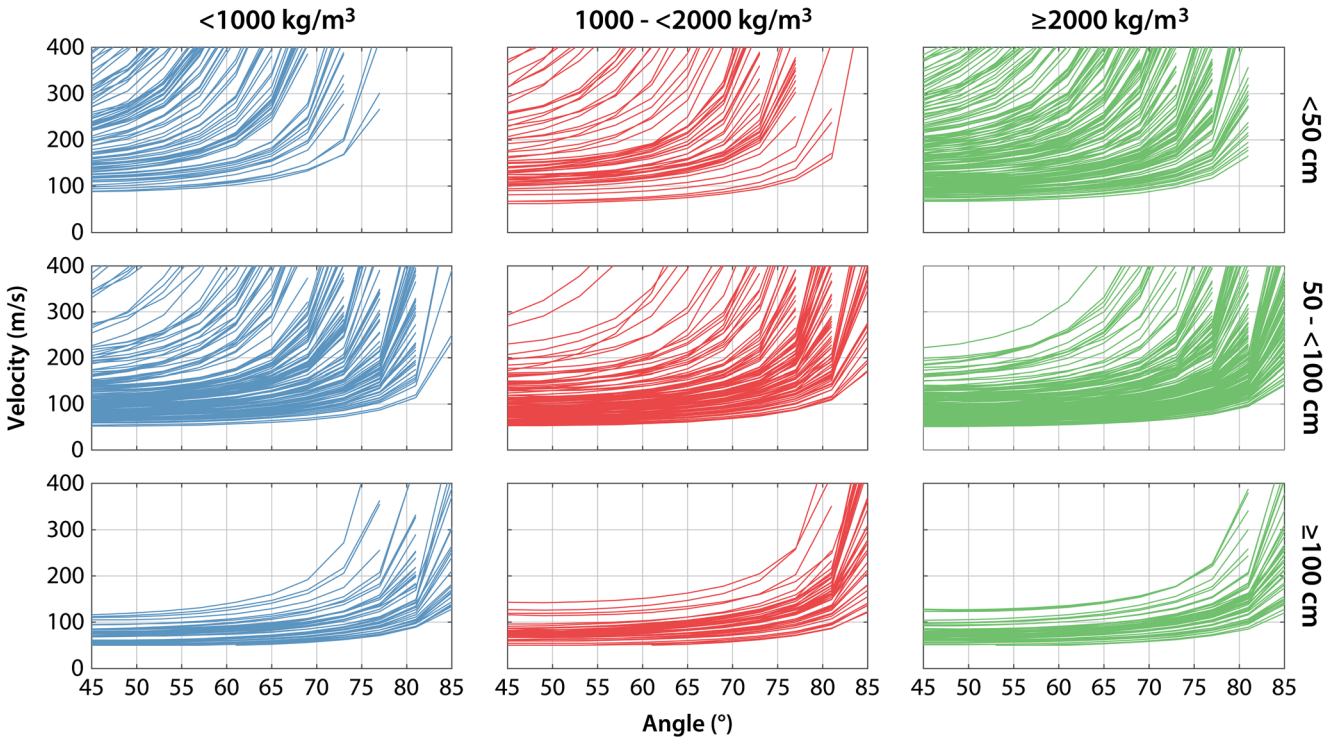

Fig. 9 Modeled block ejection velocity versus launch angle for all size and density groups. Each *curve* represents the combinations of initial velocity and launch angle that project a given block to the distances measured in the field

Table 2 Summary of ejection velocities (in m/s and calculated for an angle of 45°) for each of the nine size and density categories

Size range (cm)		<1000 kg/m^3	1000–<2000 kg/m^3	≥2000 kg/m^3
<50	p5	100	80	83
	p25	147	114	112
	p50	**221**	**150**	**159**
	p75	306	270	256
	p95	485	500	440
	Range 1	159	156	144
	Range 2	**385**	**420**	**357**
50–<100	p5	63	59	57
	p25	83	79	70
	p50	**108**	**94**	**84**
	p75	153	129	108
	p95	349	208	164
	Range 1	70	50	38
	Range 2	**286**	**149**	**107**
≥100	p5	50	53	55
	p25	56	67	63
	p50	**70**	**74**	**71**
	p75	81	82	83
	p95	111	120	124
	Range 1	25	15	20
	Range 2	**61**	**67**	**69**

5th, 25th, 50th, 75th, and 95th percentiles correspond to p5, p25, p50, p75, and p95, respectively. Range 1 = p75–p25; range 2 = p95–p5.

Bold entries highlight the median velocity (p50) and spread in velocity (Range 2) discussed in the text

Instead, the directional polylobate contours, especially for the larger blocks that were less susceptible to the moving volcanic and atmospheric gases (see next section), are most easily interpreted as the deposits of multiple sectorial-confined explosions especially directed towards the south of the vent. A greater number of explosions directed towards the south is supported by the presence of a more continuous pumice lapilli bed in the southern (inferred upwind) region (Fig. S2 in the Online Resource).

The pumiceous dacites represent the only component group that is evenly distributed in the northwest to northeast region, but this population is composed predominantly of blocks <75 cm in diameter. We propose that these smaller and low-density clasts were preferentially influenced by wind advection during the explosions. It is impossible to know the near-surface wind field during the time of Episode IV (especially since the timing of its commencement and duration are unknown), but currently the wind blows from the south/southwest during 50% of the summer months.

Constraints on modeled ejection velocity and angle

The modeling results and inverse correlation between block size and landing distance suggest that not all of the Episode IV blocks followed ballistic trajectories that were decoupled from the volcanic and atmospheric gases (Self et al. 1980; Sparks et al. 1997). Instead, they were subject to varying aerodynamic drag forces throughout three stages of flight. In the first stage, the blocks experience partial coupling with expanding magmatic volatiles within the shallow conduit. Subsequently, they enter the envelope of air overlying the vent that is displaced by the explosions and thus also moving outwards. Ballistic blocks experience reduced drag during these two stages due to lower relative velocities between the blocks and the ambient gas flow field (Fagents and Wilson 1993; Mastin 2001; de' Michieli Vitturi et al. 2010). In the final stage, the blocks are then transported through the ambient atmosphere which can be stationary or subject to a wind field. The drag forces during this stage would thus depend on that wind field (Waitt et al. 1995; Alatorre-Ibargüengoitia and Delgado-Granados 2006). We reiterate that these variations were not included in our model calculations, but their influences can still be seen in the results.

There is a complex relationship between the aerodynamic properties (i.e., size, shape, and density) of a clast and how much drag forces vary according to the medium that it travels through. We assumed a spherical shape in our model calculations and discuss below the role of block size and density. Crucial shifts in the model results for the intermediate-size class indicate a change in the magnitude of the surrounding

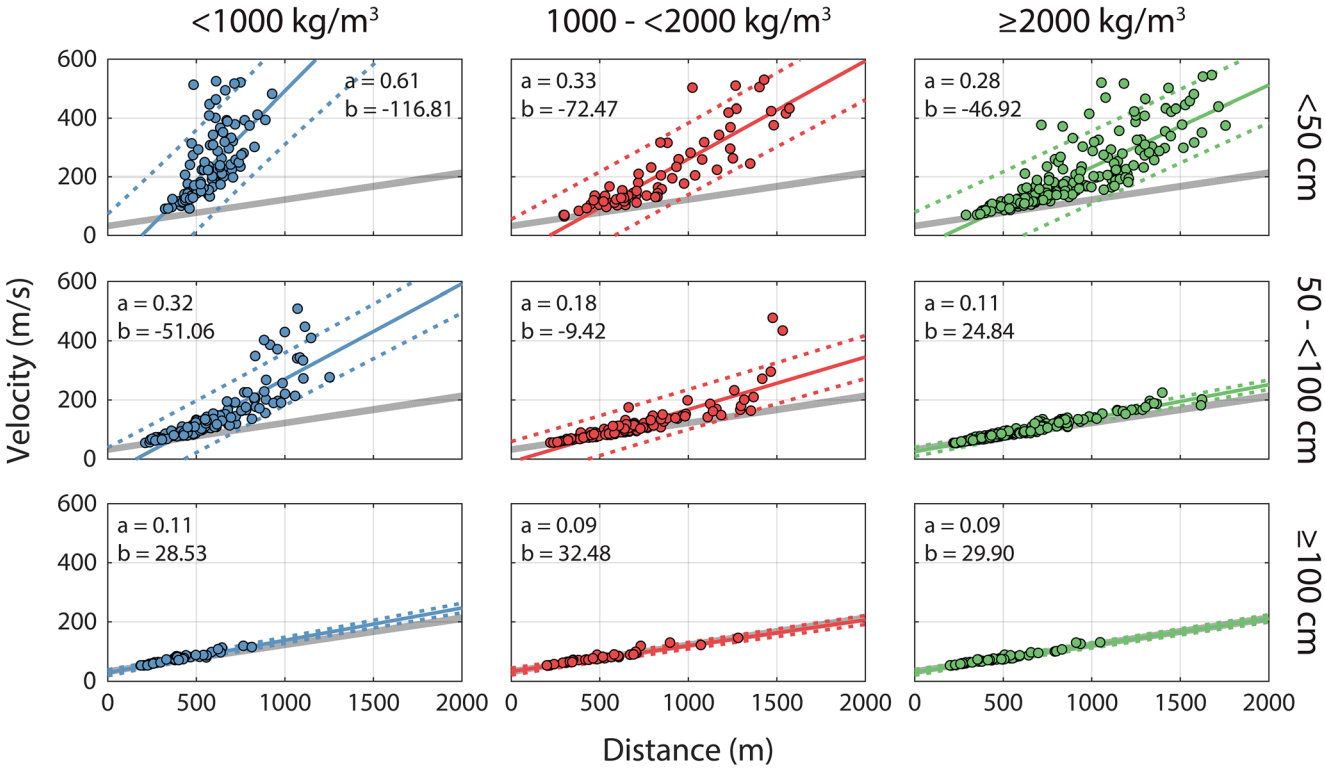

Fig. 10 Launch velocity versus ejection distance for an ejection angle of 45°, overlain by the best linear fit (*solid line*, a = slope, b = intercept) and 95% confidence interval (*dotted lines*). The *gray-shaded region* represents the 90% confidence interval of a linear fit performed on all blocks with diameters >1 m. Note how more blocks fall within this region with increasing size and density

medium's influence on block trajectory. Relative to the results for the smallest blocks, the median velocity decreases, the spread in velocity narrows, and a linear relationship between velocity and distance develops as the density increases (Figs. 9 and 10). This suggests that the smaller and low-density clasts with high exit velocities are more readily influenced by the ambient flow field, suggesting that a more complex treatment of their aerodynamics is necessary in order to properly model their trajectories. This also applies to the 297 small and/or low-density blocks with long landing distances that the model could not replicate with a range of plausible ejection velocities. We interpret the gray-shaded region in Fig. 10 to represent the most accurate velocity versus distance relationship for our blocks traveling through a still atmosphere. The model results for blocks that lie outside this region cannot be trusted and do not accurately reflect the true exit conditions throughout Episode IV. Only minor variation in the largest clasts' modeled median and spread in velocities (Fig. 9) suggests they are minimally influenced by ambient motion. Their ratio of surface area to volume is lower, thus drag per unit mass is much lower, and so the largest blocks are capable of maintaining their inertia.

We used the *Eject!* model (Mastin 2001) to assess the influence of the presence of a region of reduced drag by comparing the horizontal distance reached by particles (i) in a stationary atmosphere and (ii) in using a region of reduced drag with a radius above the vent of 200 m. Ejection velocity and angle were set at 100 m/s and 45°, respectively, and various sizes, shapes, and densities were considered. Although the definition of the region of reduced drag as considered by Mastin (2001) is somewhat arbitrary, results suggest that such a region with a 200-m radius has a greater effect on block travel distances for irregular shapes (cubes), smaller sizes (<1 m), and lower densities (<1000 kg/m^3; Fig. S3 in the Online Resource). While our *Eject!* model runs illustrate how drag forces are dependent on the particle's shape (Alatorre-Ibargüengoitia and Delgado-Granados 2006; Bagheri and Bonadonna 2016; Bertin 2017), cubes are likely to overestimate the drag. Our results emphasize that velocities estimated using a still-air calculation are most accurate for the largest size class within the Episode IV blocks.

Within individual density/diameter subsets (Fig. 9), the range between the highest and the lowest ejection velocities for a given angle is related to a combination of (1) size and density within each group, (2) distance blocks traveled, and (3) relative landing elevation (the difference between projection and landing elevations). A direct relationship between velocity and distance is confirmed in Fig. 10. The blocks in the smallest size class spanned a much larger range of distances than the larger classes (Tables 1 and 2). Additionally, elevation varied irregularly but radially around vent, and so blocks commonly traveled equivalent

Table 3 Examples of componentry described in the Vulcanian literature

Block lithology		Novarupta, 1912	Ngauruhoe, 1975	Tokachi-dake, 1988–1989	Soufrière Hills, 1996–1997							Guagua Pichincha, 1999
		This study; Adams et al. 2006	Nairn and Self 1978[a]	Yamagishi and Feebrey 1994[a]	Robertson et al. 1998[b]	Druitt et al. 2002[c]	Kennedy et al. 2005[d]	Clarke et al. 2007[d]	Burgisser et al. 2010[d]	Giachetti et al. 2010[d]	Wright et al. 2007[a]	
Non breadcrusted	Pumice/ vesiculated	X	X	X		X	X	X	X	X		
	Banded	X					X		X	X		X
	Dense juvenile	X	X	X		X		X	X	X		X
	Breccia	X		X	X		X					
	Dense lithic	X	X		X	X						
Breadcrusted		X	X	X					X	X		X

[a] Componentry is for ballistic ejecta which has been distinguished from concurrent or subsequent pyroclast fall and flow deposits

[b] Dense and brecciated lithic clasts are inferred from vent-clearing Vulcanian explosions; vesicular to dense juvenile material erupted in subsequent sustained explosive eruptions

[c] Pyroclastic fall ejecta, including both ballistic and material from plume and umbrella clouds

[d] These textures are recognized only in pyroclastic flow deposits

distances but landed at different elevations. The narrowing of the range of velocities with increasing block size can be related to (1) narrowing of the range of landing distances and (2) block size converging on a critical mass at which drag has a minimal influence.

The broad range of launch angles across which ejection velocity is relatively consistent for the largest and densest blocks suggests that angle was not a significant influence on their trajectories. Combined with the widening of the range of velocities at higher angles, these model results may indicate that the high velocity/high angle combinations are likely unrealistic conditions for most of the largest blocks.

Discussion

Eruptive conditions at Novarupta and comparisons with historical Vulcanian eruptions

We estimate a total volume of 2×10^5 m^3 DRE for the Episode IV deposit by calculating the volume of blocks within each isopleth and then adding a rough volume estimate for the lapilli component in the far field, which was approximated by isopachs of 10 and 1 cm. This corresponds to 73% ballistics and 27% lapilli fall. An ash-sized component was not included in this calculation because there is no evidence that the plume(s) contained a significant fines population. This volume equates to a hemispherical surficial dome diameter of 90 m or, alternatively, assuming a conduit radius of 10 m, a plug length of 600 m. More plausibly, based on componentry, the explosions tapped a combination of a smaller dome and a smaller part of the underlying conduit, thus these numbers are maxima. We can be sure that explosions reached into the conduit due to the presence of the Episode I dense vitrophyre blocks, but these estimates of dimensions suggest that only the shallowest regions were tapped. In contrast, pressure estimates for Vulcanian activity at Soufrière Hills have been used to suggest explosions evacuated to conduit depths of ≥2 km (Druitt et al. 2002; Melnik and Sparks 2002; Clarke et al. 2007; Burgisser et al. 2011).

Adams et al. (2006a) speculated that Episode IV involved cyclic activity of lava production and disruption, but could not conclude definitively that there was more than one explosion according to their block maps. We suggest that each of the lobes defined from isopleth information represents the products of at least one discrete explosion. It is possible that any lobe equates to more than one explosion; however, we estimate a minimum of 8–14 explosions from the number of lobes within the 125- and 75-cm isopleths, respectively (Fig. 7). This would equate to an average volume of $1.4–2.5 \times 10^4$ m^3 DRE per explosion, which is roughly an order of magnitude smaller than other well-documented Vulcanian events. For example, each of

the 88 Vulcanian explosions at Soufrière Hills volcano, Montserrat, in 1997 discharged an average of 3×10^5 m^3 of magma (Druitt et al. 2002). Nine "cannon-like explosions" at Ngauruhoe, New Zealand, on February 19, 1975, produced a total of 2.0×10^6 m^3 DRE of ejecta (Nairn and Self 1978), which averages to 2.2×10^5 m^3 per explosion. This also suggests that individual explosions during Episode IV disrupted the conduit fill to only shallow depths.

Transport and sedimentation processes during Episode IV contrasted with those from other transient explosions related to dome-building eruptions. In particular, the Episode IV deposit is purely a block and lapilli apron, i.e., there is no evidence of pyroclastic density currents, and there is no preserved ash fall. Pyroclastic transport throughout Episode IV was predominantly governed by ballistic trajectory of the block-sized pyroclasts.

No previous study has documented the detail of textural differences within and between component groups or calculated their relative proportions for a Vulcanian ballistic deposit. As such, the data pertaining to block lithology and proportions within the Episode IV deposit are unique when compared to other well-documented transient explosions (Table 3). For example, a brecciated ballistic component is rarely mentioned in any of the Vulcanian literature (with the exceptions of Yamagishi and Feebrey 1994 and Robertson et al. 1998) and its abundance and role has not been quantified. The proportion of brecciated blocks (by volume) is strikingly high at Novarupta, and we attribute it to a combination of Episode I vitrophyric material derived from the conduit margin and syn-eruptive lithic-free, lightly to densely welded breccias (Adams et al. 2006a).

The degree and variety of banding present in the Novarupta blocks is either not present or not documented in other deposits. Banded ejecta is recorded in recent studies (Table 3), but described only briefly as "dense parts with tabular shapes that form cm-thick streaks in a more vesicular clast" (Burgisser et al. 2010), "alternating bands of variable vesicularity" (Giachetti et al. 2010), or is not defined at all (Kennedy et al. 2005; Wright et al. 2007). However, flow banding during eruption of silicic magmas is recognized as an important indicator both of viscous and brittle deformation due to shear and of mingling of texturally differing magmas (Seaman et al. 1995; Tuffen et al. 2003; Gonnermann and Manga 2005; Tuffen and Dingwell 2005). We recognize a range of mingled textures within juvenile pyroclasts of varying densities and calculated that they represent roughly 20% by volume of the blocks at Novarupta. The existence of banded blocks of contrasting vesicularity means either (1) that these textures are the result of a single zone of magma that has undergone spatially variable shear stresses which have resulted in diverse vesiculation states and textures (Polacci et al. 2001; Gonnermann and Manga 2005) or (2) that portions of the melt with different textures and presumably ascent histories were mingled at a very late stage prior to eruption. Contrasting degrees of post-fragmentation expansion between light (vesicular) and dark (denser) bands suggests that the relevant melts had different levels of residual volatiles, which favors (2) but not (1). Previous studies have set precedents for the mingling and mixing of chemically distinct (e.g., Seaman et al. 1995; Perugini et al. 2004) and texturally diverse magmas (Seaman et al. 2009; Wright et al. 2011). We interpret the banding in Episode IV to indicate the presence of coexisting magma domains that were at varying stages of degassing and outgassing and significant mingling along the margins of these disparate magmas within the shallow conduit. While Vulcanian eruptions commonly show

Table 4 Comparison of velocities calculated for ballistic particles

Eruption(s) year(s)	Location	Style	Maximum landing distance[a] (m)	Velocity (m/s)	Reference
1968	Arenal volcano, Costa Rica	Vulcanian	5000	300–400	Fagents and Wilson 1993
1975	Ngauruhoe, New Zealand	Vulcanian	2800	220–260	Fagents and Wilson 1993
1977	Ukinrek Maars, Alaska	Phreatomagmatic	700	80–85	Fagents and Wilson 1993
1992	Crater peak vent, Mount Spurr, Alaska	Phreatomagmatic	3500	155–840	Waitt et al. 1995
1997	Soufrière Hills volcano, Montserrat	Vulcanian	1700	40–140	Clarke et al. 2002
1999	Guagua Pichincha, Ecuador	Vulcanian	800	77–100	Wright et al. 2007
1998, 2003, 2008	Popocatepétl, Mexico	Vulcanain	3700	110–210	Alatorre-Ibarguengoitia et al. 2012
2012	Upper Te Maari, New Zealand	Hydrothermal	1350	120–215	Breard et al. 2014
1888–1890	La Fossa volcano, Italy	Vulcanian	1000	100–150	Biass et al. 2016
1912	Novarupta, Alaska	Vulcanian	1300[b]	50–124	This study

[a] Maximum landing distance used in the modeling

[b] 1300 m refers to the maximum distance of the >1-m blocks (from which the velocities were extracted)

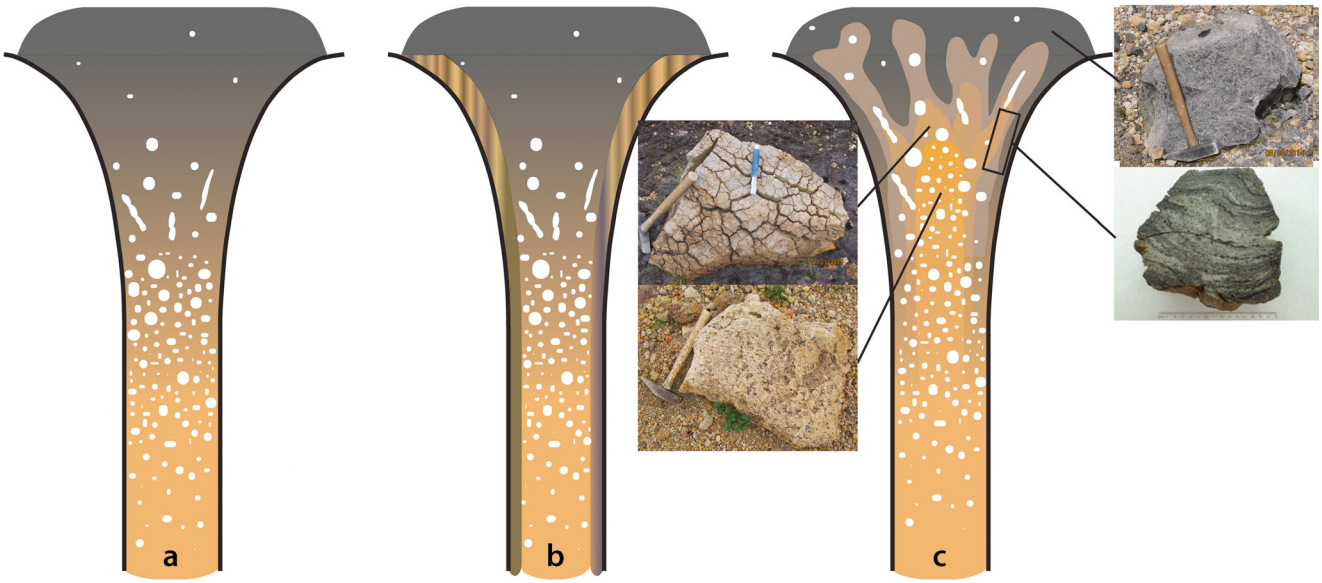

Fig. 11 Models for the shallow conduit architecture prior to Vulcanian explosions. **a** Zoned magma that is in progressively decreasing states of degassing and outgassing. **b** Vertically layered conduit with older melt along the conduit walls. **c** Complex conduit architecture involving domains of varying textures and vesiculation states. Block pictures represent the products of these melts; note how the banded blocks originated along the margins of contrasting melt domains

heterogeneities in textures, the Episode IV banded clasts appear to have experienced a very high degree of mingling without complete mixing/hybridization. We suggest this is the result of differing residence times within the upper regions of the conduit and dynamic conditions on short time scales prior to fragmentation that enabled the formation and preservation of local complex millimeter- to centimeter-scale banding between magmas of differing textures.

While breadcrusted clasts are particularly characteristic of Vulcanian eruptions, their abundance has generally not been quantified. They are typically described as a minor component within an otherwise pumice-rich deposit (e.g., Giachetti et al. 2010). In comparison, the proportion of breadcrusted blocks in the Novarupta deposit is high at 25% by number or 37% by volume. Predictably, a large proportion of the uniform and banded pumices are breadcrusted, whereas most of the breccias and dense dacites are not (Fig. 3). The banded dacite component has the highest proportion of breadcrusted blocks at 83% by volume. In this case, cracking of the dense exterior rinds on both dense and vesicular bands was likely due to the renewed vesiculation of the light-colored vesicular bands, which are conspicuously more expanded than neighboring dark, denser bands (Fig. 2g, h).

The modeling results suggest that consistent exit conditions, and presumably conduit parameters, prevailed for numerous explosions throughout Episode IV. The trajectories of the largest blocks were most reliably estimated with the model because they were minimally influenced by atmospheric motion that would have been difficult to constrain. Hence, we focus on the results for the >100-cm-size class. Our best estimated velocities range from 50 to 124 m/s with a median of ~70 m/s, which is relatively low when compared to the spectrum of velocities estimated for ballistic deposits (Table 4). This, combined with the comparatively small volume produced per explosion, could reflect relatively less energetic conditions at Novarupta—perhaps due to greater complexity within the shallow conduit. Our model velocity range is applicable across all radial sectors (i.e., does not vary with lobe direction). This implies that the multiple explosions within Episode IV consistently ejected these blocks with a narrow range of velocities, and that the conditions that prompted an explosion did not vary substantially across the multiple events within this phase.

Implications and comparisons with respect to other Vulcanian eruptions

Conduit heterogeneity prior to Vulcanian explosions is generally modeled in the form of zoned magma that exhibits progressively decreasing states of degassing and outgassing and thus displays an orderly change in textures and densities with decreasing depth (e.g., Druitt et al. 2002; Melnik and Sparks 2002; Clarke et al. 2007; Wright et al. 2007; Burgisser et al. 2010; Giachetti et al. 2010). Other authors have proposed an approximately vertical layering of the conduit, e.g., Kennedy et al. (2005) suggest that their banded and brecciated clasts originated from the conduit margin and the homogeneous pumice fragments came from the conduit center. Alternatively, Cassidy et al. (2015) proposed that a form of vertical layering develops when gas-rich magma rises rapidly

through a slowly ascending gas-poor magma located along the conduit walls. Instead of a simple layering, our data support the model proposed by Adams et al. (2006a) of a complex architecture within the shallow conduit involving both the juxtaposition of domains of contrasting texture and vesiculation state and the mingling of different textures on much shorter vertical and horizontal length scales (Fig. 11). Three key observations indicate that textural domains occurred on a range of scales: (1) the existence of uniform blocks, each representative of a single component type, which are up to >10 m in length, implies domains of at least these dimensions; (2) entire isopleth lobes dominated by blocks of a single lithology suggest that the largest domains may be even larger than the dimensions of these largest blocks; whereas (3) the banded blocks indicate mingling occurred locally on millimeter to centimeter scales. In regards to (2), lobes consisting of a single component group may have tapped small individual regions in the conduit whereas multiple component lobes either formed by more than one explosion and/or tapped a particularly complex or larger region of the conduit. As highlighted above, the banded blocks are indicative of dynamic conditions within the conduit probably along the margins of individual domains (Fig. 11).

General implications for modeling ballistic block trajectories

Two types of ballistic blocks have been proposed within the literature: (1) those that are influenced by the motions in the vent, eruption column, and ambient atmosphere and (2) those that are not (Self et al. 1980; Sparks et al. 1997). The first type of blocks require modeling transport through an expanding and decelerating gas stream and estimates of appropriate drag coefficients in order to accurately calculate their trajectories. A simpler model can be used to approximate the trajectories of blocks that are not influenced by ambient motion. However, the distinction between these two types of blocks is not clear; for example, where is the threshold, in terms of size or density, at which complex versus simple models must be applied? The answer to this question depends on the energy of the explosion, amount of volcanic gas and ash (or plume density), and the atmospheric conditions.

Our modeling results suggest that the ballistic trajectories of all blocks with diameters ≥1 m projected through a low-density, ash-poor plume produced by relatively low-energy explosions can be modeled without significant influence by the medium that they travel through. The eruption conditions throughout Episode IV differ from many of those in Table 4 in terms of shorter travel distances, reduced plume density, and weaker explosivity leading to reduced exit velocities. In addition, a greater influence of the expanding gas phase and convective plume on block trajectories might be expected for more energetic eruptions.

The Episode IV data suggest that the thresholds below which ballistic particles are influenced by motions of the surrounding medium are relatively high. Blocks <1 m and <2000 kg/m^3 fall in a transitional regime where their range is influenced by the expanding magmatic volatiles, the weak convecting plume, the envelope of air overlying the vent that is displaced by the explosion, and the ambient atmosphere. This result may in part reflect the weak energetic conditions inferred at Novarupta but perhaps has a broader application and requires modeling of the background flow field in order to accurately estimate block trajectories.

Conclusions

The Episode IV block apron and its significant textural diversity, despite chemical homogeneity, suggests that magma domains of varying degrees of degassing and outgassing were juxtaposed within the shallow conduit, with intimate mingling occurring along the margins of these domains. Some magma was newly arrived within the conduit, and possibly had not equilibrated at the depth of fragmentation as suggested by significant post-fragmentation expansion within breadcrusted pumiceous dacite and banded blocks. Our data suggest that the ejecta of Episode IV are the product of multiple explosions. These explosions tapped small portions of the conduit (horizontally and vertically), with many events directing ejecta towards the south of the vent. Block trajectory modeling revealed that ejection velocities were relatively low at 50–124 m/s, with a median of 70 m/s, and were consistent over a broad range of launch angles. The modeling results were used to establish a size and density threshold between blocks that could be modeled with a simple ballistic trajectory and those that required a more complex treatment of motions within the surrounding gaseous medium. Cumulatively, the field data and modeling results provide insight into conditions within the conduit during the critical transition from effusion to transient explosions at Novarupta that is a part of an overall downscaling from powerful steady Plinian explosions to lava effusion. To better understand the conduit fill, it will be necessary to assess the microvesicular textures of the blocks and to measure residual water contents. In particular, water contents could have implications for depths of fragmentation, degrees of degassing, and whether or not volatiles were able to diffuse between bands (during mingling) prior to fragmentation.

Acknowledgements This research was funded by the National Science Foundation grant EAR13-48080 with additional support from the Don Richter Memorial Fund. Special thanks to Tim Orr, Ed Llewellin, Hannah Azouz, and Jaclyn Guenther for assistance with field work. We would also like to thank (1) Alexa Van Eaton and an anonymous reviewer for their helpful suggestions and (2) Stephen Self for constructive and thoughtful editing.

References

Adams NK, Houghton BF, Fagents SA, Hildreth W (2006a) The transition from explosive to effusive eruptive regime: the example of the 1912 Novarupta eruption. Alaska Geol Soc Am Bull 118:620–634

Adams NK, Houghton BF, Hildreth W (2006b) Abrupt transitions during sustained explosive eruptions: examples from the 1912 eruption of Novarupta. Alaska Bull Volcanol 69:189–206. doi:10.1007/s00445-006-0067-4

Alatorre-Ibargüengoitia MA, Delgado-Granados H (2006) Experimental determination of drag coefficient for volcanic materials: calibration and application of a model to Popocatépetl volcano (Mexico) ballistic projectiles. Geophys Res Lett 32. doi:10.1029/2006GL026195

Alatorre-Ibargüengoitia MA, Delgado-Granados H, Dingwell DB (2012) Hazard map for volcanic ballistic impacts at Popocatépetl volcano (Mexico). Bull Volcanol 74:2155–2169. doi:10.1007/s00445-012-0657-2

Alatorre-Ibargüengoitia MA, Scheu B, Dingwell DB, Delgado-Granados H, Taddeucci J (2010) Energy consumption by magmatic fragmentation and pyroclast ejection during Vulcanian eruptions. Earth Planet Sci Lett 291:60–69. doi:10.1016/j.epsl.2009.12.051

Bagheri G, Bonadonna C (2016) Aerodynamics of volcanic particles: characterization of size, shape, and settling velocity. In: Mackie S, Cashman K, Ricketts H, Rust A, Watson M (eds) Volcanic ash. Elsevier, Amsterdam, pp 39–52

Benage MC, Dufek J, Degruyter W, Geist D, Harpp K, Rader E (2014) Tying textures of breadcrust bombs to their transport regime and cooling history. J Volcanol Geotherm Res 274:92–107. doi:10.1016/j.jvolgeores.2014.02.005

Biass S, Falcone JL, Bonadonna C, Di Traglia F, Pistolesi M, Rosi M, Lestuzzi P (2016) Great Balls of Fire: A probabilistic approach to quantify the hazard related to ballistics — A case study at La Fossa volcano, Vulcano Island, Italy. J Volcanol Geotherm Res 325:1–14. doi:10.1016/j.jvolgeores.2016.06.006

Bertin D (2017) 3-D ballistic transport of ellipsoidal volcanic projectiles considering horizontal wind field and variable shape-dependent drag coefficients. J Geophys Res 122:1125–1151. doi:10.1002/2016JB013320

Burgisser A, Arbaret L, Druitt TH, Giachetti T (2011) Pre-explosive conduit conditions of the 1997 Vulcanian explosions at Soufrière Hills Volcano, Montserrat: II. Overpressure and depth distributions. J Volcanol Geotherm Res 199:193–205. doi:10.1016/j.jvolgeores.2010.11.014

Burgisser A, Poussineau S, Arbaret L, Druitt TH, Giachetti T, Bourdier J-L (2010) Pre-explosive conduit conditions of the 1997 Vulcanian explosions at Soufrière Hills Volcano Montserrat: I. Pressure and vesicularity distributions. J Volcanol Geotherm Res 194:27–41. doi:10.1016/j.jvolgeores.2010.04.008

Cassidy M, Cole PD, Hicks KE, Varley NR, Peters N, Lerner AH (2015) Rapid and slow: varying magma ascent rates as a mechanism for Vulcanian explosions. Earth Planet Sci Lett 420:73–84. doi:10.1016/j.epsl.2015.03.025

Christiansen RL, Peterson DW (1981) Chronology of the 1980 eruptive activity. In: Lipman PW, Mullineaux DR (Eds.), The 1980 eruptions of Mount St. Helens, Washington. U.S Geol Surv Prof Pap 1250:17–31

Clarke AB (2013) Unsteady explosive activity: vulcanian eruptions. In: Fagents SA, Gregg TKP, Lopes RMC (Eds.). Modeling volcanic processes. Camb. Univ. Press, pp. 129–152

Clarke AB, Neri A, Voight B, Macedonio G, Druitt TH (2002a) Computational modelling of the transient dynamics of the August 1997 Vulcanian explosions at Soufrière Hills Volcano, Montserrat: influence of initial conduit conditions on near-vent pyroclastic dispersal, in: Druitt, T.H., Kokelaar, B.P. (Eds.), The eruption of Soufrière Hills Volcano, Montserrat, from 1995 to 1999. Geol Soc Lond, pp. 319–348.

Clarke AB, Ongaro TE, Belousov A (2015) Vulcanian eruptions. In: Sigurdsson H, Houghton BF, McNutt SR, Rymer H, Stix J (Eds.). The encyclopedia of volcanoes. Acad. Press, pp. 505–518

Clarke AB, Stephens S, Teasdale R, Sparks RSJ, Diller K (2007) Petrologic constraints on the decompression history of magma prior to Vulcanian explosions at the Soufrière Hills volcano Montserrat. J Volcanol Geotherm Res 161:261–274. doi:10.1016/j.jvolgeores.2006.11.007

Clarke AB, Voight B, Neri A, Macedonio G (2002b) Transient dynamics of vulcanian explosions and column collapse. Lett Nat 415:897–901. doi:10.1038/415897a

Coombs ML, Eichelberger JC, Rutherford MJ (2000) Magma storage and mixing conditions for the 1953–1974 eruptions of Southwest Trident volcano, Katmai National Park Alaska. Contrib Mineral Petrol 140:99–118

de' Michieli, Vitturi M, Neri A, Esposti Ongaro T, Lo Savio S, Boschi E (2010) Lagrangian modeling of large volcanic particles: application to Vulcanian explosions. J Geophys Res 115. doi:10.1029/2009JB007111

Diller K, Clarke AB, Voight B, Neri A (2006) Mechanisms of conduit plug formation: implications for vulcanian explosions. Geophys Res Lett 33. doi:10.1029/2006GL027391

Druitt TH, Young SR, Baptie B, Bonadonna C, Calder ES, Clarke AB, Cole PD, Harford CL, Herd RA, Luckett R, Ryan G, Voight B (2002) Episodes of cyclic Vulcanian explosive activity with fountain collapse at Soufrière Hills Volcano, Montserrat. In: Druitt TH, Kokelaar BP (Eds.). The eruption of Soufrière Hills Volcano, Montserrat, from 1995 to 1999. Geol Soc Lond, pp. 281–306

Fagents SA, Wilson L (1993) Explosive volcanic eruptions-VII the ranges of pyroclasts ejected in transient volcanic explosions. Geophys J Int 113:359–370. doi:10.1111/j.1365-246X.1993.tb00892.x

Fierstein J, Hildreth W (1992) The plinian eruptions of 1912 at Novarupta, Katmai National Park, Alaska. Bull Volcanol 54:646–684. doi:10.1007/BF00430778

Fudali RF, Melson WG (1971) Ejecta velocities, magma chamber pressure and kinetic energy associated with the 1968 eruption of Arenal volcano. Bull Volcanol 35:383–401. doi:10.1007/BF02596963

Giachetti T, Druitt TH, Burgisser A, Arbaret L, Galven C (2010) Bubble nucleation, growth and coalescence during the 1997 Vulcanian explosions of Soufrière Hills Volcano. Montserrat J Volcanol Geotherm Res 193:215–231. doi:10.1016/j.jvolgeores.2010.04.001

Gonnermann HM, Manga M (2005) Flow banding in obsidian: a record of evolving textural heterogeneity during magma deformation. Earth Planet Sci Lett 236:135–147. doi:10.1016/j.epsl.2005.04.031

Hildreth W (1987) New perspectives on the eruption of 1912 in the Valley of Ten Thousand Smokes, Katmai National Park Alaska. Bull Volcanol 49:680–693. doi:10.1007/BF01080359

Hildreth W, Fierstein J (2000) Katmai volcanic cluster and the great eruption of 1912. Geol Soc Am Bull 112:1594–1620. doi:10.1130/0016-7606(2000)112<1594:KVCATG>2.0.CO;2

Hildreth W, Fierstein J, (2012) The Novarupta-Katmai eruption of 1912: largest eruption of the twentieth century: centennial perspectives. U.S. Geol. Surv. Prof. Pap. 1791

Hoblitt RP, Wolfe EW, Scott WE, Couchman MR, Pallister JS, Javier D (1996) The preclimatic eruptions of Mount Pinatubo, June 1991. In: Newhall CG, Punongbayan RS (eds) Fire and mud: eruptions and lahars of Mount Pinatubo. Philippines. Univ. Wash. Press, Seattle, WA, pp 457–511

Houghton BF, Wilson CJN, Fierstein J, Hildreth W (2004) Complex proximal deposition during the Plinian eruptions of 1912 at Novarupta. Alaska Bull Volcanol 66:95–133. doi:10.1007/s00445-003-0297-7

Kennedy BM, Spieler O, Scheu B, Kueppers U, Taddeucci J (2005) Conduit implosion during Vulcanian eruptions. Geology 33:581–584. doi:10.1130/G21488.1

Mastin LG (2001) A simple calculator of ballistic trajectories for blocks ejected during volcanic eruptions. U.S. Geol. Surv. Open-File Rep. 01–45 16

Melnik O, Sparks RSJ (2002) Dynamics of magma ascent and lava extrusion at Soufrière Hills Volcano. Montserrat Geol Soc Lond Mem 21:153–171. doi:10.1144/GSL.MEM.2002.021.01.07

Melnik O, Sparks RSJ (1999) Nonlinear dynamics of lava dome extrusion. Nature 402:37–41. doi:10.1038/46950

Minakami T (1942) On the distribution of volcanic ejecta. (Part 1) the distributions of volcanic bombs ejected by the recent explosion of Asama. Bull Earthq Res Inst

Nairn IA, Self S (1978) Explosive eruptions and pyroclastic avalanches from Ngauruhoe in February 1975. J Volcanol Geotherm Res 3:39–60

Nguyen CT, Gonnermann HM, Houghton BF (2014) Explosive to effusive transition during the largest volcanic eruption of the 20th century (Novarupta 1912, Alaska). Geology 42:703–706. doi:10.1130/G35593.1

Perugini D, Ventura G, Petrelli M, Poli G (2004) Kinematic significance of morphological structures generated by mixing of magmas: a case study from Salina Island (southern Italy). Earth Planet Sci Lett 222:1051–1066. doi:10.1016/j.epsl.2004.03.038

Polacci M, Papale P, Rosi M (2001) Textural heterogeneities in pumices from the climactic eruption of Mount Pinatubo, 15 June 1991, and implications for magma ascent dynamics. Bull Volcanol 63:83–97. doi:10.1007/s004450000123

Robertson R, Cole P, Sparks RSJ, Harford C, Lejeune AM, McGuire WJ, Miller AD, Murphy MD, Norton G, Stevens NF, Young SR (1998) The explosive eruption of Soufrière Hills Volcano, Montserrat, West Indies, 17 September, 1996. Geophys Res Lett 25:3429–3432. doi:10.1029/98GL01442

Sahetapy-Engel ST, Harris AJL, Marchetti E (2008) Thermal, seismic and infrasound observations of persistent explosive activity and conduit dynamics at Santiaguito lava dome Guatemala. J Volcanol Geotherm Res 173:1–14. doi:10.1016/j.jvolgeores.2007.11.026

Scheu B, Kueppers U, Mueller S, Spieler O, Dingwell DB (2008) Experimental volcanology on eruptive products of Unzen volcano. J Volcanol Geotherm Res 175:110–119. doi:10.1016/j.jvolgeores.2008.03.023

Scheu B, Spieler O, Dingwell DB (2006) Dynamics of explosive volcanism at Unzen volcano: an experimental contribution. Bull Volcanol 69:175–187. doi:10.1007/s00445-006-0066-5

Seaman SJ, Dyar MD, Marinkovic N (2009) The effects of heterogeneity in magma water concentration on the development of flow banding and spherulites in rhyolitic lava. J Volcanol Geotherm Res 183:157–169. doi:10.1016/j.volgeores.2009.03.001

Seaman SJ, Scherer EE, Standish JJ (1995) Multistage magma mingling and the origin of flow banding in the Aliso lava dome, Tumacacori Mountains, southern Arizona. J Geophys Res 100:8381–8398. doi:10.1029/94JB03260

Self S, Keinle J, Huot J-P (1980) Ukinrek maars, Alaska, II. Deposit and formation of the 1977 craters. J Volcanol Geotherm Res 7:39–65

Self S, Wilson L, Nairn IA (1979) Vulcanian eruption mechanisms. Nature 277:440–443

Sparks RSJ, Bursik MI, Carey SN, Gilbert JE, Glaze L, Woods AW (1997) Volcanic Plumes. Wiley, New York

Tuffen H, Dingwell D (2005) Fault textures in volcanic conduits: evidence for seismic trigger mechanisms during silicic eruptions. Bull Volcanol 67:370–387. doi:10.1007/s00445-004-0383-5

Tuffen H, Dingwell DB, Pinkerton H (2003) Repeated fracture and healing of silicic magma generate flow banding and earthquakes? Geology 31:1089–1092. doi:10.1130/G19777.1

Turcotte DL, Ockendon H, Ockendon JR, Cowley SJ (1990) A mathematical model of vulcanian eruptions. Geophys J Int 103:211–217. doi:10.1111/j.1365-246X.1990.tb01763.x

Waitt RB, Mastin LG, Miller TP (1995). Ballistic showers during Crater Peak eruptions of Mount Spurr Volcano, summer 1992. In: Keith TEC (Ed.). The 1992 eruptions of Crater Peak vent, Mount Spurr Volcano, Alaska. U.S Geol Surv Bull B-2139, pp. 89–106

Wilson L (1972) Explosive volcanic eruptions-II. The atmospheric trajectories of pyroclasts. Geophys J Int 30:381–392. doi:10.1111/j.1365-246X.1972.tb05822.x

Woods AM (1995) A model of vulcanian explosions. Nucl Eng Des 155:345–357. doi:10.1016/0029-5493(94)00881-X

Wright HMN, Cashman KV, Rosi M, Cioni R (2007) Breadcrust bombs as indicators of Vulcanian eruption dynamics at Guagua Pichincha volcano Ecuador. Bull Volcanol 69:281–300. doi:10.1007/s00445-006-0073-6

Wright HMN, Folkes CB, Cas RAF, Cashman KV (2011) Heterogeneous pumice populations in the 2.08-Ma Cerro Galán Ignimbrite: implications for magma recharge and ascent preceding a large-volume silicic eruption. Bull Volcanol 73:1513–1533. doi:10.1007/s00445-011-0525-5

Yamagishi H, Feebrey C (1994) Ballistic ejecta from the 1988-1989 andesitic Vulcanian eruptions of Tokachidake volcano, Japan: morphological features and genesis. J Volcanol Geotherm Res 59:269–278